ADVANCED MATERIALS
www.advmat.de

Self-Amputating and Interfusing Machines

*Bilige Yang, Amir Mohammadi Nasab, Stephanie J. Woodman, Eugene Thomas, Liana G. Tilton, Michael Levin, and Rebecca Kramer-Bottiglio**

Biological organisms exhibit phenomenal adaptation through morphology-shifting mechanisms including self-amputation, regeneration, and collective behavior. For example, reptiles, crustaceans, and insects amputate their own appendages in response to threats. Temporary fusion between individuals enables collective behaviors, such as in ants that temporarily fuse to build bridges. The concept of morphological editing often involves the addition and subtraction of mass and can be linked to modular robotics, wherein synthetic body morphology may be revised by rearranging parts. This work describes a reversible cohesive interface made of thermoplastic elastomer that allows for strong attachment and easy detachment of distributed soft robot modules without direct human handling. The reversible joint boasts a modulus similar to materials commonly used in soft robotics, and can thus be distributed throughout soft robot bodies without introducing mechanical incongruities. To demonstrate utility, the reversible joint is implemented in two embodiments: a soft quadruped robot that self-amputates a limb when stuck, and a cluster of three soft-crawling robots that fuse to cross a land gap. This work points toward future robots capable of radical shape-shifting via changes in mass through autotomy and interfusion, as well as highlights the crucial role that interfacial stiffness change plays in autotomizable biological and artificial systems.

1. Introduction

Many biological organisms can adapt their morphology and behavioral control policy toward changing tasks and environments.[1] Among examples of such adaptive morphology,[2–4] two particularly striking methods are self-amputation[5] and dynamic aggregation (interfusion).[6] Self-amputation, or autotomy, is the ability for animals to amputate appendages to escape danger.[5] For example, lizards will voluntarily cast off a tail if seized by a predator[7] and crabs shed injured appendages that might otherwise hinder their movement.[8] In a colony of insects (especially ants), biologists have observed and characterized the dynamic aggregation of individuals and how such aggregation aids in functional behaviors through a collective arrangement of morphologies.[6,9] For example, by rearranging the mechanical connection between individual ants, an ant colony can link up to form a bridge to cross a gap on the forest floor or form into the shape of a ball to float on water.[10,11] Both autotomy and aggregation are functional methods of shape change that require the subtraction or addition of mass, and prior works suggest that especially subtractive inspirations are often overlooked for synthetic systems.[12,13]

A key functional feature that enables both self-amputation and dynamic aggregation in animals is the ability to form and break connections, both within a body (individual scale) and between bodies (group scale) (**Figure 1A**). On the individual scale, biological autotomy tells us that the intentional separation of appendages is achieved by actively adjusting the tensile strength along a predetermined fracture plane that connects extremities and the rest of the body,[14–17] and animals lacking control of this fracture plane cannot autotomize.[7,18] On the group scale, there are clear ties between animals that connect/disconnect and modular robotics. Myriad options for reversible connections exist for rigid-material modular robots, enabling adaptive body configurations and controls under changing circumstances.[19] In parallel, emerging soft robots also promise adaptability to changing tasks and environments.[1] The intersection of soft and modular robots offers soft modular robots,[20] which are made of predominantly soft materials and require equally soft reversible joints that do not interfere with the novel functions afforded by body compliance.

Many connectors for soft robots rely on mechanical forces and include simple linkages like metal pins,[21] plastic sockets,[22] screws and bolts,[23] and push fittings.[24] These connectors have high strength due to strong mechanical coupling but require precise alignment and manual handling to connect. More importantly, the rigid materials used in these structures reduce the overall flexibility and compliance of the soft system.

B. Yang, A. M. Nasab, S. J. Woodman, E. Thomas, L. G. Tilton, R. Kramer-Bottiglio
School of Engineering & Applied Science
Yale University
9 Hillhouse Avenue, New Haven, CT 06511, USA
E-mail: rebecca.kramer@yale.edu
M. Levin
Department of Biology
Allen Discovery Center at Tufts University
200 Boston Ave. Suite 4604, Medford, MA 02155, USA
M. Levin
Wyss Institute for Biologically Inspired Engineering
Harvard University
3 Blackfan Cir, Boston, MA 02115, USA

The ORCID identification number(s) for the author(s) of this article can be found under https://doi.org/10.1002/adma.202400241

DOI: 10.1002/adma.202400241

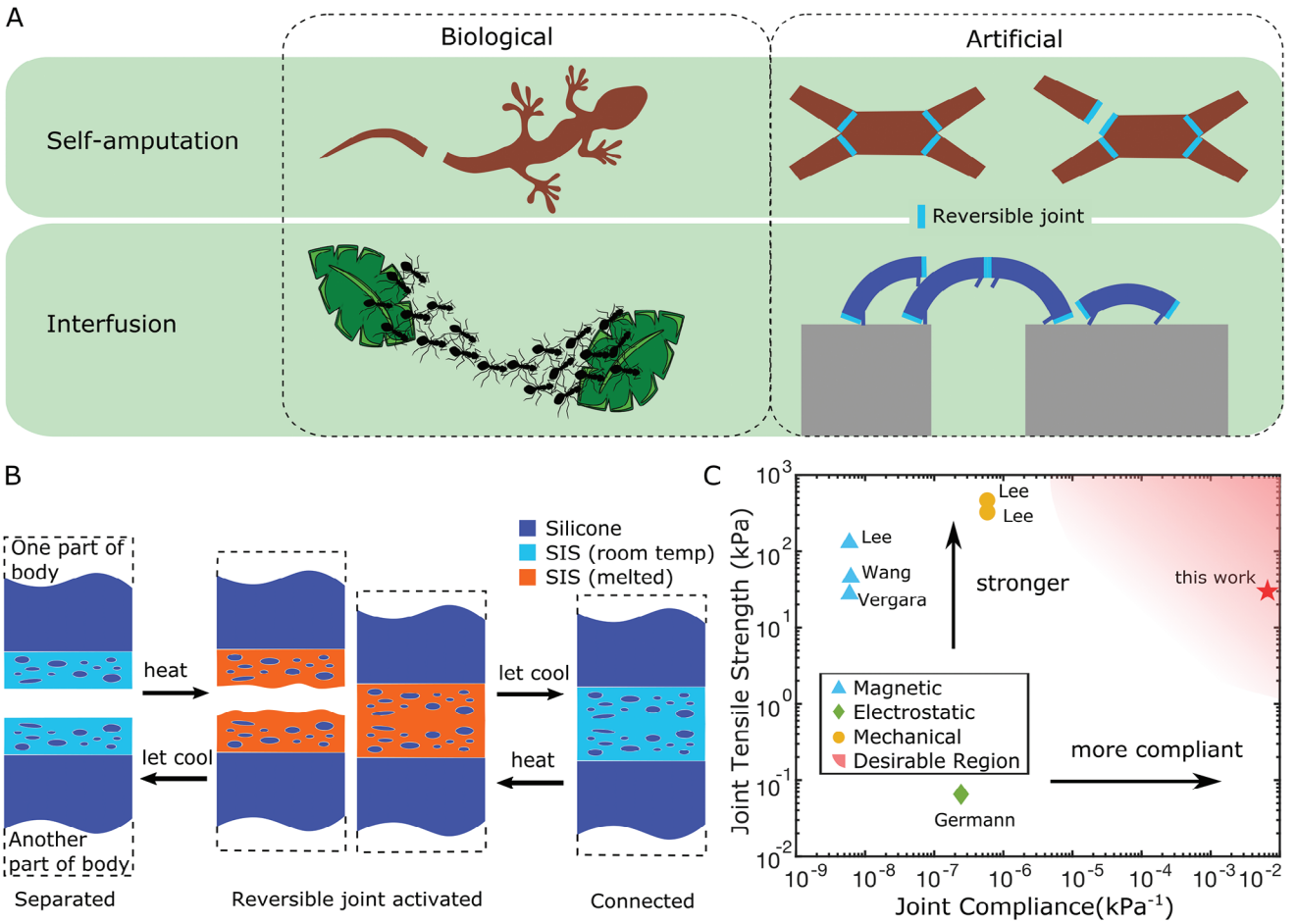

Figure 1. Overview of the reversible joint concept. A) Self-amputation and interfusion in biological systems and their artificial counterparts. B) Schematic for the structure and mechanism of the reversible joint. C) Joint tensile strength versus joint compliance for relevant connection mechanisms in the literature. The mechanical[24] and magnetic connectors[25,27,28] are strong but stiff, while the electrostatic connector[31] is compliant but weak. An ideal reversible joint is both strong and compliant.

Magnetic forces have also been utilized to create connection mechanisms for soft robots.[25–28] By embedding permanent magnets into the outside surfaces of soft bodies, soft modules can snap together and establish a strong magnetic bond. Yet magnets also introduce undesired rigidity and weight into the soft system. Furthermore, the magnetic force is typically constant or challenging to modulate, and large attractive forces often require manual manipulation with the risk of tearing the soft materials. Electromagnets can produce a reversible magnetic force but face similar disadvantages of rigidity and weight, and have thus far only been applied to rigid modular robots.[29,30]

Several additional connective mechanisms exist that may offer advantageous compliance in the context of soft robotics. Electrostatic force can be generated between thin membranes with conductive carbon traces under high voltage.[31] Even though the system can remain soft, electroadhesion is several orders of magnitude weaker than the aforementioned mechanical and magnetic connections, making electroadhesion suitable only for extremely light modules. Micro-patterning the surface of soft structures creates dry adhesives for soft modules based on van der Waals interactions.[32] However, van der Waals connections are still relatively weak (compared to magnetic and mechanical connectors) as well as limitingly directional, and detachment can require manual manipulation. Wang et al. illustrated the feasibility of using hot-melt adhesives, a type of thermoplastic polymer, as a reversible connection for pick-and-place applications.[33] Relatedly, Huang et al. showed a programmable adhesive hydrogel that can attach and detach conductive objects via the application of voltage.[34] López-Díaz et al. also showed a hydrogel-based connection that uses hydration-triggered self-healing for reversible adhesion capacity, although the connection time given therein is 24 h.[35] These approaches lack cool-state compliance, applicability to non-conductive materials, and sufficiently rapid connective reversibility, respectively. However, such prior works point toward an emerging category of stimuli-responsive reversible adhesives suitable for integration with soft robots for programmable self-amputation, interfusion, and reconfiguration.

Herein, we introduce a novel material architecture using thermally responsive thermoplastic elastomer for the attachment and detachment of soft robot components or bodies. We considered the following requirements: 1) Tunable bonding strength (high for attachment and low for detachment); 2) Many attach/detach

cycles without substantial performance degradation; and 3) Compliance matching to common structural materials in the soft robotics literature. Using a bi-continuous structure of thermoplastic elastomer as the basis for our approach, we characterize the formulation and geometry to optimize the reversible joint for the requirements above. Further, we prove the utility of the reversible joint in autotomizing and interfusing soft robot demonstrations.

2. Results

2.1. Bicontinuous Thermoplastic Foam (BTF) as a Soft Reversible Joint

We achieved a temperature-modulated reversible joint based on a bicontinuous thermoplastic foam structure. The thermoplastic used in this work is styrene-isoprene block copolymer (SIS), which is a rubbery solid at room temperature (≈25 °C) and melts into a liquid at elevated temperature (≈140 °C). We sought to utilize the heat-tunable strength of SIS for an artificial joint that could be broken off and rejoined based on temperature—a "reversible joint." To achieve such a joint, we first plasticized SIS with paraffin oil to suppress its modulus into a range representative of silicones commonly used in soft robotics, e.g., Dragon-Skin 10,[36] as well as decrease its melting point (see details in Experimental Section). SIS does not inherently bond to silicones and urethanes, so we devised a bicontinuous foam structure comprised of an SIS scaffold infused with a silicone matrix (Figure 1B and Experimental Section), which we termed Bicontinuous Thermoplastic Foam (BTF). This foam structure allows SIS to melt and combine with its counterpart on another soft body cohesively while still adhering to the silicone matrix (and the rest of the soft robotic body) via mechanical bonding (Figure 1B).

Reversible connections are accomplished as follows. Two silicone bodies each have a layer of BTF on their exposed surfaces. The foams are heated above the melting point of SIS, such that the SIS in the BTF melts into a viscous liquid. The silicone matrix in the BTF holds the molten SIS like a sponge, preventing it from flowing out. Upon contact between two BTF surfaces (without requiring direct pressure), the molten SIS from both sides combines into a continuous liquid mass due to the cohesive force between SIS molecules. As the joint cools, the SIS solidifies, connecting the silicone bodies. To disconnect, the joint is heated such that the SIS melts and weakens substantially. The two sides of the joint are then easily separated. Even after separation, each side retains its bicontinuous structure of SIS in a silicone scaffold, which enables multiple repeated connections.

An ideal joint for soft modular robots, beyond facilitating reversible connections, would exhibit high strength, cyclically stable bonds, and match the compliance of materials commonly used to make soft bodies. We conducted a comprehensive mechanical assay to evaluate the BTF joint's fit with this ideal criterion. We first conducted tensile tests on a joint to ascertain its maximum tensile strength (Figure S1, Supporting Information), a typically reported metric for other reversible connection systems. Figure 1C plots the tensile strength of the BTF joint (29.5 kPa, SD = 0.395 kPa) along with several other joints used for soft bodies as a function of their joint compliance. The connection strength of the BTF joint was 454× greater than that of the electrostatic joint,[31] and even on par with rigid connectors such as magnetic joints[25] and mechanical joints.[24] The BTF joint boasts both high strength and high compliance, as indicated by its position in the upper right corner of Figure 1C. One reported mechanical joint also falls toward the desired target of high strength and high compliance,[24] but the joint cannot be softened for disconnection, limiting its utility for modular soft robotic applications.

We also conducted T-peel tests as a representative loading condition for soft joints used on robot systems (subjecting them to a combination of tensile and shear stresses). T-peel tests were carried out with BTF joint samples (five for each condition) cast atop an inextensible fabric-reinforced silicone substrate (**Figure 2A**). At room temperature (25 °C), the joint exhibited an average bond strength of 6.84 N cm^{-2} (68.4 kPa, SD = 9.61 kPa). With a suppressed melting temperature of T_m = 115 °C due to plasticization (see Figure S2, Supporting Information Text, and Experimental Section), heating the joint to a disconnection temperature of 120 °C decreased its bond strength by more than 30×, to 0.21 N cm^{-2} (2.1 kPa, SD = 1.25 kPa) (Figure 2B). Tests at an intermediate disconnection temperature of 65 °C yielded an average bond strength of 0.53 N cm^{-2} (5.3 kPa, SD = 1.26 kPa) (Figure 2B). The proximity of the peak force at an intermediate temperature to that above the SIS melting temperature suggests that we do not always need to heat to above the T_m to facilitate disconnection. Indeed, probing the force response between 25 and 65 °C reveals a rapid and monotonic decrease in peak forces in this temperature range (Figures S3 and S4, Supporting Information).

2.2. Performance Variation with Thickness and Pore Size

To understand the influence of key design variables on the resulting bond strength of the reversible joint, we conducted further T-peel tests on BTF specimens varying thickness per side, *t*, and average pore size of the SIS foam, *d* (Figure 2A,C,D). The maximum stress a joint can sustain at 25 and 65 °C roughly increased with an increase in the thickness of the joint (Figure 2C). This finding is consistent with literature documenting the effect of the thickness on the peel strength of adhesive joints.[37] Namely, as the joint thickness increases, a larger volume of polymer is subjected to deformation per unit area of detachment, increasing the total work expended while peeling. Past the T_m of SIS at 120 °C, the maximum stress stayed approximately constant as joint thickness increased, and we thus speculate that the separation force of the liquid–liquid interface does not vary with the change in bulk thickness.[38] Collectively, the T-peel results reveal that the ratio between the bond strengths at room temperature and above T_m is positively correlated with *t*.

To further understand the strength of the connection during peeling, we constructed a 2D finite element model implementing a J-integral method where a constant force is applied to the joint to calculate the energy release rate (G) at the tip of an edge crack (see Figure S5, Supporting Information). G is proportional to the square of the model-I fracture toughness (K_I): $G = \frac{K_I^2}{E}$.[39] A lower G means that the joint will tear at a higher maximum force. The simulation showed that, as joint thickness increased, G decreased for the room-temperature BTF joint. For SIS foam at 120 °C, the simulation predicted increasing G with increasing

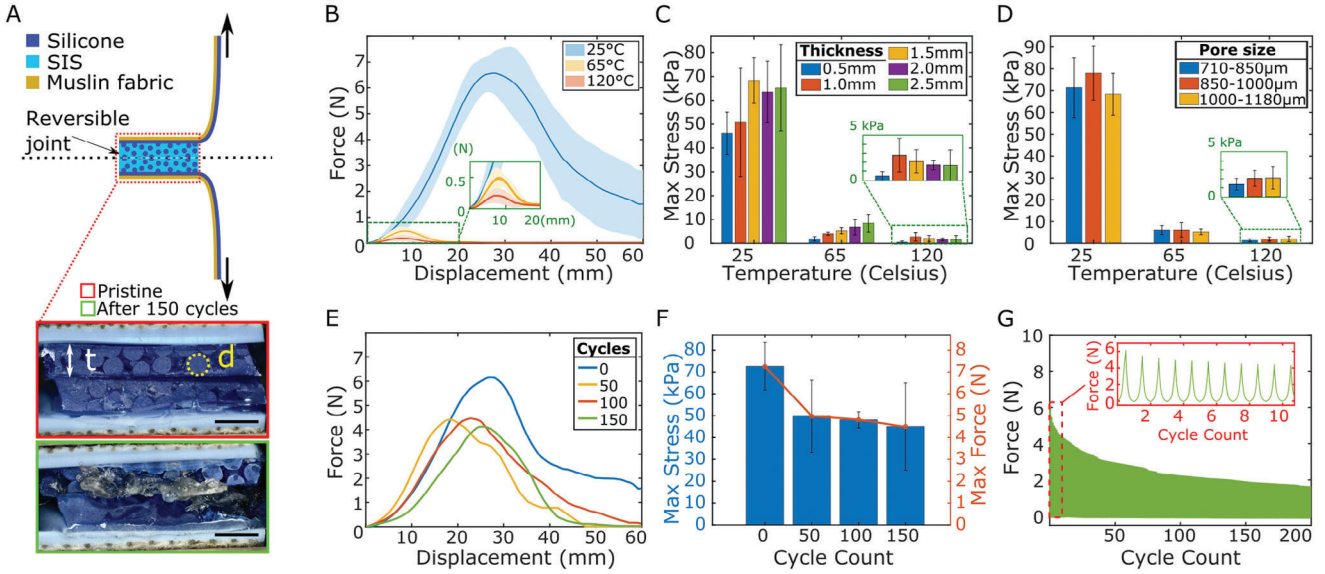

Figure 2. Mechanical characterization of the bicontinuous thermoplastic foam (BTF) reversible joint. A) A schematic of the T-peel test setup. (*Inset*) Microscope images of the reversible joint before and after 150 cycles of "heat-connect-cool-heat-disconnect." The round circles are the silicone network, while the SIS network fills the space between the circles. The bright blue bars on the top and bottom are the silicone substrate. t is the thickness of the BTF on one side. d is the pore size of the SIS foam. Scale bar, 2 mm. B) Force response of reversible joint for standard samples of 1 cm^2 contact area and 1.5 mm thickness at 25, 65, and 120 °C. Error clouds are one SD over five samples. C) Maximum sustained stress for joint samples of different thicknesses at different temperatures, while holding pore size range at 850–1000 μm. Error bars are one SD over five samples. D) Maximum sustained stress for joint samples of different pore sizes of the SIS foam at different temperatures, holding thickness constant at 1.5 mm. Error bars are one SD. E) Representative force response of joint standard samples of 1 cm^2 contact area and 1.5 mm thickness after cyclic (dis)connections. Additional samples and averages are provided in Figure S6 (Supporting Information). F) Maximum sustained force and stress of joints after cyclic (dis)connections. Error bars are one SD over three samples. G) Force response of a joint under a cyclic displacement of 14 mm at room temperature.

thickness, which was consistent with the experimental results showing a slight decline in the pull-off force (Figure 2C).

Pores in the SIS foam were created with sacrificial sugar particles and later filled in by silicone (see Experimental Section and Figure S2, Supporting Information). The sacrificial sugar particles were infused with packing density $\phi = 0.74$ across all samples.[40] Pore sizes are normally an important determinant of the mechanical properties of foams.[41–43] We were surprised, then, to find that varying pore size had minimal effect on the maximum stress sustained by the BTF joint (Figure 2D). Several studies in the literature also report that varying pore size does not affect the strength of foams, granted the porosity (packing fraction of pores) is held constant.[44,45] Consequently, streamlined manufacturing of the material structure is possible using larger particles that are much easier to incorporate into the host SIS material.

2.3. Cyclic Strength and Repeatability

Having quantified the impact of key design parameters on the reversible joint's adhesion strength, we proceeded to characterize the cyclic performance. Two tests were conducted. First, to see how repeated connection and disconnection affects joint strength, we conducted experiments containing a series of steps: 1) heating up two sides of the joint to connect, 2) contacting, and cooling down to firm up the connection, and 3) heating up the joint again to disconnect. We did the above steps over 0 (pristine), 50, 100, and 150 cycles and tested the final cooled-down joint strength by pulling it to failure (Figure 2E,F). Figure 2E shows representative force responses, while averages across multiple samples (N = 3) are given in Figure S6 (Supporting Information). The ultimate strength of the joint decreased with increasing cycle number but still remained at 67% of the pristine maximum force after 150 cycles. After 150 cycles, a portion of the melted SIS exited the silicone matrix, causing gradual connection degradation (inset of Figure 2A). Most deterioration of the joint happened within the first 50 cycles and thereafter degradation slowed (Figure 2F). Extrapolating past cycle 150 (based on a linear approximation after cycle 50), we predict that the joint can hold 50% of its original strength at around cycle 250. For most systems that are designed with a safety factor of 2, 50% of the initial strength keeps the system operational. Further, since morphological adaptation enabled by connection and disconnection is unlikely to be a frequent functional need, we believe that joints operational through 250 cycles are sufficient for most soft modular robots.

For the second cyclic test, we sought to evaluate the behavior of the joint when it experienced repeated loading in its cool, connected phase. We conducted cyclic tests for which we repeatedly subjected the room temperature joint to a fixed displacement and recorded the resulting holding force. Figure 2G shows one representative sample, while additional samples and averages are given in Figure S7 (Supporting Information). We started with a

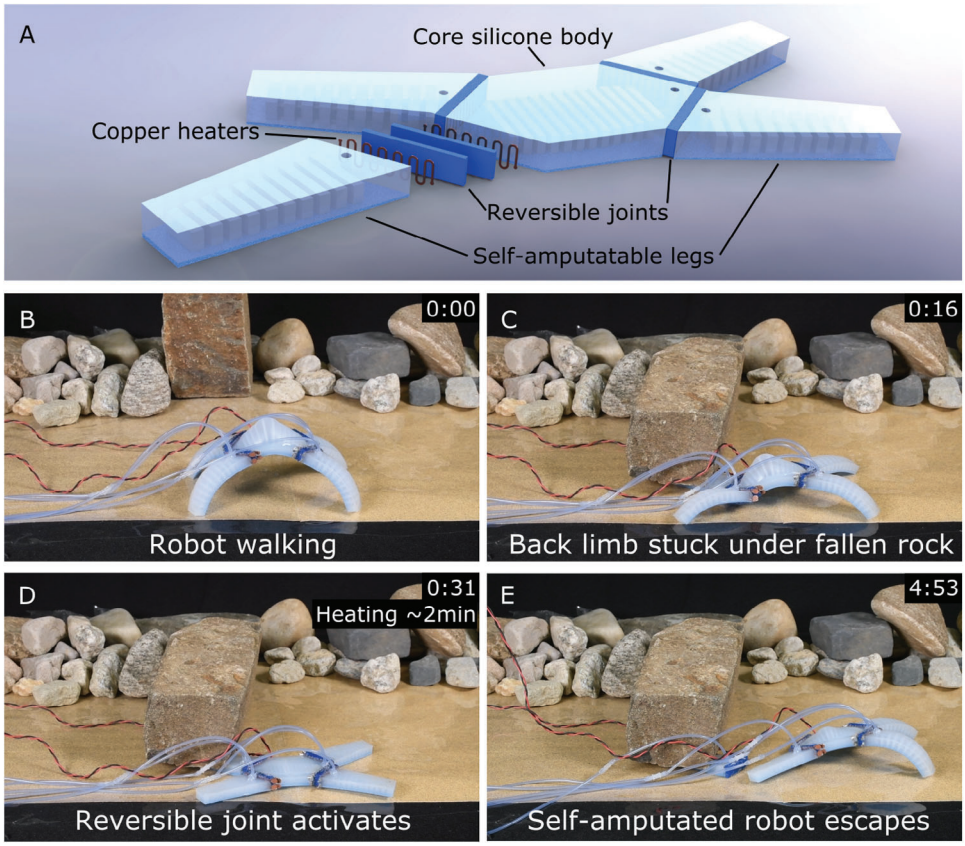

Figure 3. A soft quadruped robot performing self-amputation. A) A schematic of the quadruped robot equipped with reversible joints and copper heaters. The robot is 12 cm long and 7 cm wide. B) The robot walked in an unstructured environment. C) A rock unexpectedly fell onto the back limb of the robot, trapping the robot. D) One reversible joint was weakened via Joule heating of the copper heater. E) The robot kept walking and left the stuck limb behind.

14 mm displacement at the joint, which corresponds to the joint's initial maximum peel load or 6 N (on average). After 50 and 200 cycles, the joint held a force of 2.5 N (≈40% of initial) and 1.4 N (≈25% of initial), respectively. Conducting the same test with a smaller displacement of 12 mm (see Figure S7, Supporting Information), which corresponds to 55% of the maximum peel load or 3.60 N, we find that after 200 cycles, the joint held 1.17 N (32.5% of the force at the start). Therefore, we deduce that even smaller displacements weaken the joint under large (>200) cycle numbers.

Having verified the mechanical strength and cyclic stability of the reversible joint, we moved to assess its application in modular soft robotic systems.

2.4. Self-Amputation of a Soft Quadruped Robot

We showcase a soft robot, an adaptation of the well-known soft quadruped robot introduced by Shepherd et al.,[46] equipped with reversible joints navigating an environment with pre-planned hazards (Movie S1, Supporting Information). Between the limbs and torso of the soft robot, reversible soft joints were added together with a flexible copper heater (**Figure 3**A). The robot was teleoperated via a direct line of sight. Under undisturbed conditions, the robot walked forward (Figure 3B). Subjected to an adverse condition—having part of the body pinned beneath a heavy object (Figure 3C)—the robot was able to self-amputate a limb to escape via heating of the thermally responsive joint (Figure 3D,E). After the self-amputation, the robot walked away as a three-legged robot. This demonstration shows the effectiveness of on-demand joints for the adaptability and autonomy of robots facing unstructured and hazardous environments.

In unstructured environments, abundant contaminants may interfere with joint functionality. To test joint robustness, we deliberately exposed the melted interface to soil and water, respectively, and measured bond strength afterward (Figure S8, Supporting Information). We found that bond strength decreased by only 6% after soil contact and by 20% after water soaking. These tests demonstrate the suitability of our on-demand joints for real-world environments.

2.5. Interfusion for Collaborative Robots

Environments can engender hazardous conditions that are difficult for single artificial units to navigate. The ability to connect and disconnect on-demand benefits a group of robots aiming to complete a task that is impossible for a single robot (Movie S2, Supporting Information). We constructed a group of soft crawlers with reversible joints at their ends (**Figure 4**A) and built a

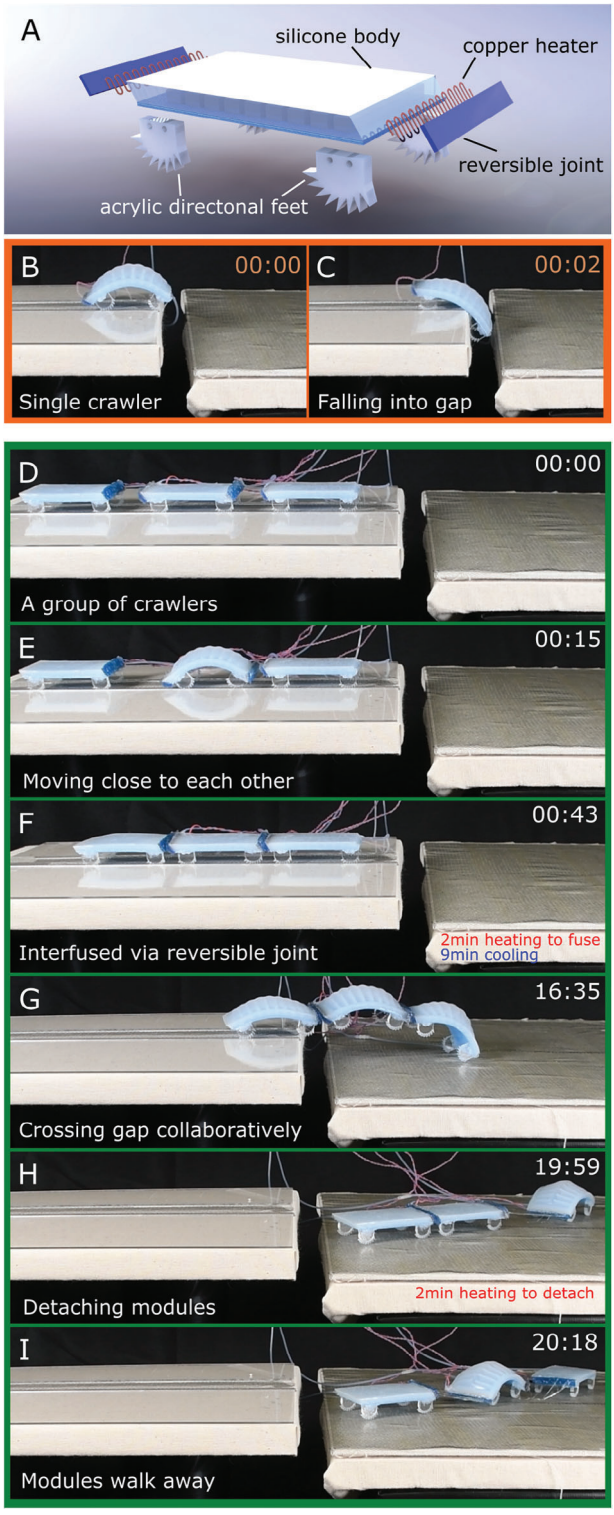

Figure 4. A cluster of interfusing soft crawlers. A) A schematic for the soft crawler (with an actuator body), equipped with reversible joints and copper heaters on both ends. The crawler is 7 cm long and 4 cm wide. B,C) A single crawler could crawl on flat ground but fell into a gap that is too wide to cross. D–I) A cluster of crawlers interfused with each other, and then crossed the gap collaboratively. After the crossing, the reversible joints were heated up again to release individual modules so they again operate independently.

locomotion course with a gap in the path. A single soft crawler was effective at locomoting on flat ground. Yet, when faced with the wide crevice, it failed to cross and dropped into the gap (Figure 4B,C). However, a group of robots with reversible joints could interfuse and collaborate to cross the gap. Three crawlers first lined up, one behind another (in contact), by crawling forward, and then the soft joints were heated to connect with their neighbors (Figure 4D–F). After the joints cooled and strengthened, the crawlers collectively walked over the gap by utilizing the added length of the body (Figure 4G). After the crossing was complete, the joints were heated again to detach, and the modules walked away separately (Figure 4H,I). This demonstration shows how reversible joints can enable soft modular robots with independent and collective behaviors. The soft robotic modules are capable of joining with other modules to make use of an editable anatomy, and also capable of continued task performance independently if cut off from the main body, which is a prodigious feat of dynamic plasticity that can counteract the effects of unexpected experiences or damage.

3. Conclusion

In this work, we observed the general principle that a reversible joint is key to realizing certain shape-based adaptations in biological organisms. The ability to voluntarily sever appendages when encountering danger is a survival skill for a wide range of animals, as is the ability to dynamically aggregate for collective function. Both approaches underscore the importance of reversible joints in biological adaptation, either as an individual or as a collective.

We see potential for soft artificial systems with reversible joints for shape change via mass addition and subtraction. This work is the first instantiation of a fully soft reversible joint, which enabled a self-amputating robot and an interfusing system of robots. The reversible joint presented herein boasts inactive compliance and strength similar to common elastomers and active weakening for easy separation. Moreover, such synthetic systems can shed light on the algorithms used by multiscale natural biological systems in which structure, size, and composition change dynamically (e.g., the collective cell behavior of embryonic morphogenesis in multicellular creatures, metamorphosis, remodeling, and cancer).[47,48]

Mechanically, our reversible joint can bear 68.4 kPa (6.84 N per 1 cm^2 contact area) at room temperature, which is much stronger than benchmark compliant joints (17.5× that of van der Waals force connectors and 1052× that of electrostatic connectors), while maintaining the same compliance (modulus) as the host robot's body. At an elevated temperature (65 °C), the joint strength decreases to less than one-tenth of the original for easy detachment. We have also demonstrated repeated connection and disconnection of the joint over 250 cycles while maintaining more than 50% of its original strength. Finally, the reversible joint does not require precise alignment for attachment and detachment. A 1.5 mm thick and 1 cm^2 area BTF requires ≈400 J of energy to reach the (dis)connection temperature, promising untethered operation.

The superior performance of this reversible joint material architecture allows for a first-of-its-kind demonstration of a self-amputating soft robot that can escape from entrapment

under a rock and a group of interfusing soft crawlers that can cross a gap too wide for one alone. These demonstrations are uniquely enabled by bio-inspired fracture planes with tunable stiffness, and show that autonomy and interfusion may be promising survival mechanisms for soft robots in variable environments.

4. Experimental Section

Reversible Joint Fabrication: To decrease the melting point of polystyrene-block-polyisoprene-block-polystyrene (SIS; 432393, Sigma Aldrich) from 140 to 115 °C for easier processing, pristine SIS was plasticized with paraffin oil (18512-1L, Sigma Aldrich). Briefly, SIS pellets and paraffin oil were added to a beaker in a 60:40 ratio by weight, and the mixture was thinned with toluene (adding 2× the mixture's weight in toluene). This ratio of SIS and paraffin was selected after the initial testing of different ratios (see Appendix, Figure S9, Supporting Information). This mixture was placed on a hot plate at 80 °C for 4 h with occasional manual stirring to help the dissolution of SIS. Then the toluene was allowed to evaporate overnight, resulting in plasticized SIS. See Appendix, Figure S2 (Supporting Information) for illustration.

Plasticized SIS was fabricated into an open-cell foam using round sugar particles (SUGLETS, Colorcon) as a sacrificial material. To incorporate the sugar particles into the SIS, the SIS was kept at an elevated temperature (to suppress the SIS viscosity), with pressure applied so the SIS flowed into the gaps between the sugar particles. A cylindrical steel herb press (BouPower, Amazon) was filled with closely packed sugar and the plasticized SIS. The cylinder was then put into an oven at 120 °C for 4 h, occasionally turning the handle of the press to sustain the pressure on the SIS. The result was a disk of closely packed round sugar with SIS in between. This disk was then put into room temperature water to dissolve away the sugar overnight, yielding an open-cell foam of plasticized SIS. To finalize the bicontinuous thermoplastic foam (BTF), the SIS foam was manually pressed into pre-cure silicone (DragonSkin 10, Smooth-On). After curing, the BTF was cut into appropriate sizes with an X-ACTO knife for use as a reversible joint.

T-Peel and Cyclic Tests: For both peel and cyclic mechanical tests, a materials testing machine (Instron 3345) was used to record the force during the peeling and the distance of separation for the joints. The temperature conditions were created via a digital heat gun (N2030, Neu Master) blowing directly on the samples.

For the T-peel tests (Figure 2A–D), the speed of peeling was 60 mm min^{-1} and the samples were peeled to a displacement of 60 mm. The T-junction was made of two strips of muslin fabric (4 × 1 cm) coated in silicone (Smooth-Sil 950, Smooth-On), one being pulled upward and one downward. The silicone layer emulated a silicone-based body interface, and the muslin fabric limited the amount of stretch in the substrate to make sure deformation and breakage occurred at the joint. Each strip had a BTF layer (1 × 1 cm in contact area with various thicknesses) glued on via silicone adhesive (Silpoxy, Smooth-On). The two BTF layers were touched together while heated to 120 °C for 3 min and then cooled down to room temperature before testing. The heating step ensured that the two pieces were fused to each other.

For the cyclic tests, first, the process of "heat-connect-cool-heat-disconnect" was repeated with the BTF joint for 0, 50, 100, and 150 cycles, with four respective sets of samples. Then, the resultant joint was pulled to failure at 60 mm min^{-1} to record the maximum force (Figure 2E,F). Second, for a fused joint at room temperature, samples were repeatedly strained to a set displacement and then returned to the original state for 200 cycles (Figure 2G).

Heating and Cooling for Joint Demonstration: Copper heater: In both the soft quadruped and soft crawler demonstrations, an embedded copper coil was used to heat up the reversible joint to 120 °C for (dis)connection. This copper coil was fabricated using a ProtoLaser U4 (LPKF, Germany) to cut out a serpentine pattern on a 1 × 4 cm piece of single-sided flexible PCB Board (thickness = 0.005 in, FlexPCB, Pulsar). The resulting copper coil had a resistance of 0.8 Ω. A constant current of 2 A (input power of 3.2 W) was supplied to each joint for ≈2 min before the joint was heated to the break-off/reattach temperature (120 °C).

Cooling: To complete fusing, the joint should cool to room temperature (25 °C). The cooling time varied based on environmental conditions such as temperature and air circulation. In the laboratory tests, it was found the BTF took ≈3 min to cool. The rate of cooling depends on the BTF's surface area, with a larger surface area allowing for faster heat transfer.

Supporting Information

Supporting Information is available from the Wiley Online Library or from the author.

Acknowledgements

This work was supported by the National Science Foundation (NSF) under grant no. EFMA-1830870 and IIS-1955225, as well as by the Office of Naval Research under award N00014-21-1-2417. Any opinions, findings, and conclusions or recommendations expressed in this material are those of the authors and do not necessarily reflect the views of the Office of Naval Research. S.J.W. was supported by the NASA NSTGRO Fellowship (80NSSC22K1188).

Conflict of Interest

The authors declare no conflict of interest.

Data Availability Statement

The data that support the findings of this study are available from the corresponding author upon reasonable request.

Keywords

autotomy, modular robotics, soft robotics

Received: January 5, 2024
Revised: April 25, 2024
Published online:

[1] D. Shah, B. Yang, S. Kriegman, M. Levin, J. Bongard, R. Kramer-Bottiglio, *Adv. Mater.* **2021**, *33*, 2002882.
[2] K. Gotthard, S. Nylin, *Oikos* **1995**, 3.
[3] B. H. Robison, *Mar. Freshwater Behav. Physiol.* **1999**, *32*, 17.
[4] J. S. Reidenberg, *Anat. Rec.* **2007**, *290*, 507.
[5] T. L. Maginnis, *Behav. Ecol.* **2006**, *17*, 857.
[6] N. J. Mlot, C. A. Tovey, D. L. Hu, *Proc. Natl. Acad. Sci.* **2011**, *108*, 7669.
[7] A. R. Clause, E. A. Capaldi, *J. Exp. Zool. Comp. Exp. Biol.* **2006**, *305*, 965.
[8] Z. Emberts, C. W. Miller, D. Kiehl, C. M. St. Mary, *Behav. Ecol.* **2017**, *28*, 1047.
[9] F. J. Vernerey, T. Shen, S. L. Sridhar, R. J. Wagner, *J. R. Soc., Interface* **2018**, *15*, 20180642.
[10] S. Goss, S. Aron, J.-L. Deneubourg, J. M. Pasteels, *Naturwissenschaften* **1989**, *76*, 579.
[11] M. Tennenbaum, Z. Liu, D. Hu, A. Fernandez-Nieves, *Nat. Mater.* **2016**, *15*, 54.

[12] G. S. Adams, B. A. Converse, A. H. Hales, L. E. Klotz, *Nature* **2021**, *592*, 258.
[13] Q. T. Davis, S. Woodman, M. Landesberg, R. Kramer-Bottiglio, J. Bongard, in *2023 IEEE Int. Conf. on Soft Robotics (RoboSoft)*, IEEE **2023**, pp. 1–6.
[14] I. Wilkie, *Nat. Mater.* **1978**, *186*, 311.
[15] L. Bickell-Page, G. Mackie, *Philosophical Transactions of the Royal Society of London. Series B: Biological Sciences* **1991**, *331*, 155.
[16] I. Wilkie, *Cell Tissue Res.* **1979**, *197*, 515.
[17] K. W. Sanggaard, C. C. Danielsen, L. Wogensen, M. S. Vinding, L. M. Rydtoft, M. B. Mortensen, H. Karring, N. C. Nielsen, T. Wang, I. B. Thøgersen, J. J. Enghild, *Plos one* **2012**, *7*, e51803.
[18] W. E. Dobson, *J. Exp. Mar. Biol. Ecol.* **1985**, *94*, 223.
[19] K. Gilpin, D. Rus, *IEEE Rob. Autom. Lett.* **2010**, *17*, 38.
[20] C. Zhang, P. Zhu, Y. Lin, Z. Jiao, J. Zou, *Adv. Intell. Syst.* **2020**, *2*, 1900166.
[21] M. A. Robertson, J. Paik, *Sci. Rob.* **2017**, *2*, 9.
[22] S. Kurumaya, B. T. Phillips, K. P. Becker, M. H. Rosen, D. F. Gruber, K. C. Galloway, K. Suzumori, R. J. Wood, *Soft Rob.* **2018**, *5*, 399.
[23] Z. Jiao, C. Ji, J. Zou, H. Yang, M. Pan, *Adv. Mater. Technol.* **2019**, *4*, 1800429.
[24] J.-Y. Lee, W.-B. Kim, W.-Y. Choi, K.-J. Cho, *IEEE Rob. Autom. Lett.* **2016**, *23*, 30.
[25] A. Vergara, Y.-s. Lau, R.-F. Mendoza-Garcia, J. C. Zagal, *PloS one* **2017**, *12*, e0169179.
[26] J. Zou, Y. Lin, C. Ji, H. Yang, *Soft Rob.* **2018**, *5*, 164.
[27] W. Wang, N.-G. Kim, H. Rodrigue, S.-H. Ahn, *Mater. Horiz.* **2017**, *4*, 367.
[28] J.-Y. Lee, K.-J. Cho, in *2017 14th Int. Conf. on Ubiquitous Robots and Ambient Intelligence (URAI)*, IEEE, **2017**, pp. 65–67.
[29] P. Moubarak, P. Ben-Tzvi, *Rob. Auton. Syst.* **2012**, *60*, 1648.
[30] B. T. Kirby, B. Aksak, J. D. Campbell, J. F. Hoburg, T. C. Mowry, P. Pillai, S. C. Goldstein, in *2007 IEEE/RSJ Int. Conf. on Intelligent Robots and Systems*, IEEE, **2007**, pp. 2787–2793.
[31] J. Germann, M. Dommer, R. Pericet-Camara, D. Floreano, *Adv. Rob.* **2012**, *26*, 785.
[32] Y. A. Tse, S. Liu, Y. Yang, M. Y. Wang, in *2020 3rd IEEE Int. Conf. on Soft Robotics (RoboSoft)*, IEEE, **2020**, pp. 150–155.
[33] L. Wang, F. Iida, *IEEE/ASME Trans. Mechatron.* **2012**, *18*, 1397.
[34] J. Huang, Y. Liu, Y. Yang, Z. Zhou, J. Mao, T. Wu, J. Liu, Q. Cai, C. Peng, Y. Xu, B. Zeng, W. Luo, G. Chen, C. Yuan, L. Dai, *Sci. Rob.* **2021**, *6*, 53.
[35] A. López-Díaz, J. De La Morena, F. Ramos, E. Vázquez, A. S. Vázquez, in *2022 Int. Conf. on Robotics and Automation (ICRA)*, IEEE, **2022**, pp. 7124–7130.
[36] S. Park, K. Mondal, R. M. Treadway III, V. Kumar, S. Ma, J. D. Holbery, M. D. Dickey, *ACS Appl. Mater. Interfaces* **2018**, *10*, 11261.
[37] A. N. Gent, G. R. Hamed, *Polym. Eng. Sci.* **1977**, *17*, 462.
[38] A. Ghoufi, P. Malfreyt, D. J. Tildesley, *Chem. Soc. Rev.* **2016**, *45*, 1387.
[39] W. Soboyejo, *Mechanical Properties of Engineered Materials*, CRC Press, Boca Raton **2002**.
[40] T. C. Hales, arXiv preprint math/9811071, **1998**.
[41] N. Tuncer, G. Arslan, E. Maire, L. Salvo, *Mater. Sci. Eng., A* **2011**, *530*, 633.
[42] B. Jiang, Z. Wang, N. Zhao, *Scr. Mater.* **2007**, *56*, 169.
[43] E. Ciecierska, M. Jurczyk-Kowalska, P. Bazarnik, M. Gloc, M. Kulesza, M. Kowalski, S. Krauze, M. Lewandowska, *Compos. Struct.* **2016**, *140*, 67.
[44] X. Xia, X. Chen, Z. Zhang, X. Chen, W. Zhao, B. Liao, B. Hur, *J. Magnesium Alloys* **2013**, *1*, 330.
[45] B. van Bochove, D. W. Grijpma, *Eur. Polym. J.* **2021**, *143*, 110223.
[46] R. F. Shepherd, F. Ilievski, W. Choi, S. A. Morin, A. A. Stokes, A. D. Mazzeo, X. Chen, M. Wang, G. M. Whitesides, *Proc. Natl. Acad. Sci.* **2011**, *108*, 20400.
[47] M. Levin, *Biochem. Biophys. Res. Commun.* **2021**, *564*, 114.
[48] M. Levin, *Front. Psychol.* **2019**, *10*, 2688.